Topological domain walls in helimagnets

P. Schoenherr,[1] J. Müller,[2] L. Köhler,[3] A. Rosch,[2] N. Kanazawa,[4] Y. Tokura,[4,5] M. Garst,[2,3*] D. Meier[1,6,7*]

[1]*Department of Materials, ETH Zurich, Vladimir-Prelog-Weg 4, 8093 Zürich, Switzerland.*

[2]*Institut für Theoretische Physik, Universität zu Köln, Zülpicher Str. 77, 50937 Köln, Germany.*

[3]*Institut für Theoretische Physik, Technische Universität Dresden, Zellescher Weg 17, 01062 Dresden, Germany.*

[4]*Department of Applied Physics, University of Tokyo, Tokyo 113-8656, Japan.*

[5]*RIKEN Center for Emergent Matter Science (CEMS), Wako 351-0198, Japan.*

[6]*Department of Materials Science and Engineering, Norwegian University of Science and Technology, Sem Sælandsvei 12, NO-7034 Trondheim, Norway.*

[7]*Center for Quantum Spintronics, Department of Physics, Norwegian University of Science and Technology, NO-7491 Trondheim*

*__markus.garst@tu-dresden.de; dennis.meier@ntnu.no__

Domain walls naturally arise whenever a symmetry is spontaneously broken. They interconnect regions with different realizations of the broken symmetry, promoting structure formation from cosmological length scales to the atomic level [1,2]. In ferroelectric and ferromagnetic materials, domain walls with unique functionalities emerge, holding great promise for nanoelectronics and spintronics applications [3–5]. These walls are usually either of Ising-, Bloch-,

or Néel-type and separate homogeneously ordered domains. Here we demonstrate that a wide variety of completely new domain walls occurs in the presence of spatially modulated domain states. Using magnetic force microscopy and micromagnetic simulations, we show three fundamental classes of domain walls to arise in the near-room-temperature helimagnet iron germanium (FeGe). In contrast to conventional ferroics, the domain walls exhibit a well-defined inner structure, which – analogous to cholesteric liquid crystals – consists of topological disclination and dislocation defects. Similar to the magnetic skyrmions that form in the same material [6,7], the domain walls can carry a finite topological charge, permitting an efficient coupling to spin currents and contributions to a topological Hall effect. Our study establishes a new family of magnetic nano-objects with non-trivial topology, opening the door to innovative device concepts based on helimagnetic domain walls.

In chiral magnets the Dzyaloshinskii-Moriya interaction (DMI) twists the magnetization and leads to a helimagnetic ground state. The magnetic moments periodically wind around a certain axis, $\mathbf{Q}$, with the wavelength λ determined by red a competition between the usual exchange interaction and the DMI [8]. The overall magnetization can be visualized as a stack of equidistant sheets with uniformly oriented moments, where the orientation rotates from one sheet to the next, see Fig. 1a,b. The lamellar morphology of the chiral spin texture is thus analogous to cholesteric liquid crystals [9] and, to some extent, magnetic stripe domains [10]. The involved length scales, however, are strikingly different. In helimagnets, the characteristic periodicity is up to three orders of magnitude smaller, with lamellae having nanoscopic dimensions.

Despite this difference in length scales, one may expect that these systems develop similar type of defects [11,12]. Smooth spatial variations of the helix axis $\mathbf{Q}$ simply result in a curvature of the lamellar spin structure [13]. More pronounced variations, however, may break the periodicity and induce vortices, i.e., disclinations (Fig. 1c,d). The strength of such vortices is parametrized by the winding angle of the helix axis on a path encircling the vortex core. As the helix axis is a director ($\mathbf{Q} = -\mathbf{Q}$), half integer vortices are possible with $+\pi$ and $-\pi$ rotations (Fig. 1c,d). Furthermore, disclinations can pair up and form edge dislocations (Fig. 1e), with the Burgers vector B quantifying the distance D between them.

We reveal the fundamental importance of disclination and dislocation defects for the formation and properties of domain walls in helimagnets, presenting such walls as a magnetic analog to grain boundaries in liquid crystals. A wide variety of functional helimagnetic domain walls with non-trivial topology is observed, including the vortex domain walls recently suggested by Li *et al.* [14]. Using magnetic force microscopy (MFM) we study domain walls in the near-room-temperature chiral magnet FeGe ($T_{\mathrm{N}} = 278$ K). FeGe single crystals are grown by chemical vapour transport and their phase purity (B20) is confirmed by powder X-ray diffraction (see Methods and Supplementary Fig. S0 for details). For our MFM studies, (100)- and (110)-oriented samples with a thickness of ≈ 500 μm are cut and chemo-mechanically polished with silica slurry, yielding flat surfaces with a roughness of about 1 nm. MFM is sensitive to the out-of-plane component of the magnetic stray field, and helimagnetic order manifests as a stripe-like pattern of bright and dark lines in the MFM scans in Fig. 2a-c (corresponding topography images are presented in Supplementary Fig. S4). The periodicity of the pattern is $\lambda = 70$ nm, matching with previous bulk data [15]. However, we find equivalent values of λ on (100) and (110)-oriented surfaces, which indicates that $\mathbf{Q}$ preferentially lies within the surface plane. This orientation is different from the bulk, where $\mathbf{Q}$ orients along the $\langle 100 \rangle$ direction. The MFM data thus reflects a surface-anchoring of $\mathbf{Q}$ implying a surface reconstruction of magnetic order [16], i.e., formation of magnetic surface domains with in-plane $\mathbf{Q}$. Furthermore, the measured statistical orientational distribution of $\mathbf{Q}$ is almost flat with a slight tendency to point along a $\langle 100 \rangle$ direction (if present) within the surface plane. The observations indicate that the surface domains are largely independent of both the crystallographic orientation and bulk magnetism.

Most interestingly, the MFM scans reveal helimagnetic domain walls with a complex, but well-defined inner structure. Their structure crucially depends on the angle $\angle(\mathbf{Q}_1, \mathbf{Q}_2)$ enclosed between the helix axes of the adjacent domains as defined and summarized in Fig. 2. Based on our data we distinguish curvature walls (type I, Fig. 2a), zig-zag disclination walls (type II, Fig. 2b), and dislocation walls (type III, Fig. 2c).

Walls of type I occur for the smallest angles ($\lesssim 85°$) $\angle(\mathbf{Q}_1, \mathbf{Q}_2)$ and exhibit a smooth, continuous rotation of the helix axis from $\mathbf{Q}_1$ to $\mathbf{Q}_2$ (Fig. 2a). Type II walls display a characteristic zig-zag pattern of alternating $\pm\pi$ disclinations. They arise for intermediate $\angle(\mathbf{Q}_1, \mathbf{Q}_2)$ (Fig. 2b) and induce distortions in the helimagnetic spin structure that extend over micrometer-sized distances away from the wall. Type III walls form for large $\angle(\mathbf{Q}_1, \mathbf{Q}_2)$, involving a rather abrupt transformation from $\mathbf{Q}_1$ to $\mathbf{Q}_2$ (Fig. 2c). On a closer inspection, type III walls can be identified as a chain of magnetic edge dislocations.

The length of domain walls (type I to III) can reach several micrometers, exceeding the characteristic length scale of the helical structure, λ, by two orders of magnitude. Individual walls can also change their type and thereby adapt to local variations of $\angle(\mathbf{Q}_1, \mathbf{Q}_2)$. An example is seen in Fig. 2c, where a dislocation wall (type III) turns into a curvature wall (type I). To evaluate pinning effects, we image domain walls before and after heating above T_{N} and also record their response to magnetic fields as exemplified in Supplementary Fig. S3. The data show that domain walls tend to appear in similar positions after cooling, which we attribute to the presence of structural defects at the surface or in surface-near regions. The pinning is overcome by transiently applying a moderate magnetic field (50 mT in Supplementary Fig. S3), reflecting that the effect is rather weak. Most importantly, we observe that domain walls reappear with a different spin texture after annealing. This change shows that defects act as pinning centers for domain walls, but they do not govern their magnetic structure. Furthermore, we observe an additional constant, non-dipolar background in our MFM images wherever the helimagnetic spin structure is distorted (see bright contrast in Fig. 2). Whether this background originates from, e.g., quadrupolar magnetic fields[17] or other low-symmetry phenomena remains to be demonstrated.

Most importantly for this study, the observation of the three types of domain walls strikingly corroborates the analogy between chiral magnets and cholesteric liquid crystals, where such domain walls have been observed, too [18–20]. This universality emphasizes that the domain wall formation is governed by the inherent topology arising from the lamellar structure, being independent of the involved length scales and microscopic properties.

Figure 2d presents a quantitative analysis of more than 90 measured domain walls. The larger angle α enclosed by the domain wall and one of the helix axes $\mathbf{Q}_i$, measured within the triangle defined by $\mathbf{Q}_1$ and $\mathbf{Q}_2$ (see Fig. 2a-c), is plotted as function of $\angle(\mathbf{Q}_1, \mathbf{Q}_2)$. The data shows that, at the surface, $\mathbf{Q}$ is oriented in all directions, resulting in a broad spectrum of angles ($0^\circ \leq \angle(\mathbf{Q}_1, \mathbf{Q}_2) \leq 180^\circ$). Type I walls dominate for angles $\lesssim 85^\circ$ (red dots), type II walls are realized approximately between 85° and 140° (blue dots) and type III walls for angles $\gtrsim 140^\circ$ (green dots). Figure 2d reflects that structure and orientation of the walls are interlinked. For walls of type I and III, the angle α follows the bisecting line ($\alpha = \frac{1}{2}\angle(\mathbf{Q}_1, \mathbf{Q}_2)$). In contrast, type II walls have a tendency to orient parallel to one of the $\mathbf{Q}_i$, so that $\alpha = 90^\circ$. Close to the transition regions around 85° and 140°, we occasionally observe a special case of type II walls. This subgroup of walls exhibits a minimal distance $D = \lambda/2$ between $\pm\pi$ disclinations (light-blue dots) was previously observed in Ref. 7 and discussed theoretically in Ref. 14. Bisecting domain walls as well as zig-zag structures were also anticipated by Li *et al.*[14].

To understand the relation between the orientation of a wall and its topological magnetic structure, we perform 2D micromagnetic simulations (see also Supplementary Information). We determine the energy density for various domain walls as function of $\angle(\mathbf{Q}_1, \mathbf{Q}_2)$ on a finite size system extending up to a cut-off distance $L = 12\lambda$ away from the wall (Fig. 3). The calculations reveal that type I walls (Fig. 3a) are lowest in energy for small angles $\angle(\mathbf{Q}_1, \mathbf{Q}_2)$ (red line in Fig. 3). Type II walls with $\alpha = 90°$ (Fig. 3b) become energetically favourable as $\angle(\mathbf{Q}_1, \mathbf{Q}_2)$ exceeds $85°$, which is in excellent agreement with the experimental data (Fig. 2d).

Blue lines in Fig. 3 correspond to the energies of type II walls with varying distance D between $\pm\pi$ disclinations. The energy of a pair of π and $-\pi$ disclinations grows logarithmically with D (Ref. 9) so that for an angle $\angle(\mathbf{Q}_1, \mathbf{Q}_2) = 90°$ the energy per length of the type II domain wall scales as $\log D/D$. As a consequence, domain walls with large D are in principle preferred energetically (see Supplementary Information). In order to account for the finite D observed in the MFM images, we consider a finite cut-off length L in our simulations ($L = 12\lambda$, i.e., $D = 9\lambda/2$ in Fig. 3). For angles $\angle(\mathbf{Q}_1, \mathbf{Q}_2)$ that deviate from $90°$, the arrangement of disclinations is elastically distorted with an energy cost that grows quadratically with the deviation $\angle(\mathbf{Q}_1, \mathbf{Q}_2) - 90°$, but linearly with D. As the angle $\angle(\mathbf{Q}_1, \mathbf{Q}_2)$ increases, type II walls with smaller D are therefore energetically favoured until a defect distance of $D = 4\lambda/2$ is reached, which markes the transition from type II to type III walls. Type II walls with minimal defect distance ($D = \lambda/2$, Fig. 3c) are more costly than other configurations. Their high energy cost are in agreement with their rareness in our MFM data and their tendency to occur in transition regions (light blue dots in Fig. 2d).

At around 145° walls of type III become energetically less costly than type II walls ($D = 3\lambda/2$). Different micromagnetic wall structures are possible, all with similar energy (Fig. 3d-g). Within our numerical accuracy, a chain of serially aligned edge dislocations, first with Burgers vector $B = 3\lambda$ (see Supplementary Information) and then with $B = 2\lambda$ (Fig. 3d), is lowest in energy. Towards larger angles, type III walls with $B = 2\lambda$ and $B = \lambda$ (Fig. 3e) become almost degenerate. In addition, more complex domain wall structures with slightly higher energy arise (Fig. 3f,g). Consistent with the small energy difference, a large variety of type III walls is observed experimentally (see also Supplementary Figure S2), and the micromagnetic structure frequently changes along the wall (see Fig. 2c).

Aside from their intriguing magnetic textures, the domain walls may also carry a topological skyrmion number, which fundamentally distinguishes them from classical magnetic stripe domains and other lamellar structures. In general, the topology of a magnetic structure is identified via the topological charge density $\rho_{\mathrm{top}} = \frac{1}{4\pi}\mathbf{M}(\partial_x \mathbf{M} \times \partial_y \mathbf{M})$ for the unit vector field of the magnetization $\mathbf{M}$ defined within the (x, y) plane [21]. A single skyrmion with the magnetization pointing downwards at its centre and a topological charge $W = \int dxdy\rho_{\mathrm{top}} = -1$ is depicted in Fig. 4a. The same charge is obtained if the structure is embedded in a topologically trivial helimagnetic background as illustrated in Fig. 4b. This embedded skyrmion however is equivalent to a pair of edge dislocations with Burgers vector $B = \lambda$ (Fig. 4c,d). The dislocation with $B = \lambda$ can thus be interpreted as a single meron, i.e., a half-skyrmion, which carries charge $W = -\frac{1}{2}$. The sign reflects the orientation of the magnetization at the meron core. Straightforward generalization of this argument (see Supplementary Information for details) yields a general relation between the topological charge of a dislocation and its Burgers vector

$$W_{\text{disloc.}} = \frac{s}{2}\text{mod}_2\left(\frac{B}{\lambda}\right) \tag{1}$$

where mod_2 is the modulo 2 operation, and the sign, $s = \pm 1$, is determined by the orientation of $\mathbf{M}$ at the dislocation center.

In order to obtain the topological charge for domain walls, one has to add the charges of dislocations or, alternatively, pairs of $\pm\pi$ disclinations contained within the wall. This leads to the conclusion that type I and type III walls with continuous stripes have zero topological charge (Fig. 3a,d,e). The type III walls of Fig. 3f,g with broken stripes, however, have a finite charge W. Similarly, type II walls can have a finite or zero charge W (see also Fig. 4e). An odd dimensionless distance $2D/\lambda$ between $\pm\pi$ disclinations leads to $W \neq 0$ and an even distance to $W = 0$. Such topological textures with a finite charge $W \neq 0$ are in general expected [21,22] to give rise to an emergent electrodynamics for electrons and magnons and to contribute to a topological Hall effect [23–26].

Our results reveal a new class of magnetic spin textures with non-trivial topology and establish a striking analogy between topological domain walls in chiral magnets and defect networks in mesoscopic liquid crystals. The walls naturally arise when cooling the sample below T_{N} as domains nucleate and grow, and it can be expected that they also profoundly influence macroscopic properties. Enabled by their chiral magnetic microstructure, the walls can carry a finite charge and, hence, couple efficiently to spin currents, which is to be demonstrated in future experiments. The walls and their building blocks, the magnetic disclinations and dislocations, are likely associated with long lifetimes that play a key role for the ac susceptibility and general relaxation dynamics in helimagnets [27,28]. In particular, they might be crucial for previously observed melting processes [29,30] and the pressure-induced non-Fermi liquid behavior [31–33]. The observations apply to chiral magnets in general and reveal a large variety of topologically non-trivial magnetic nano-objects – beyond skyrmions [21,34,35] – extending the field of topology-based spintronics into the realm of helimagnetic domain walls.

Methods

Sample growth: FeGe single crystals were grown by chemical vapour transport from FeGe B35 powder with I2 (20 mg) in an evacuated quartz tube. The tube was mounted in a heated three-zone furnace for 1 month with a thermal gradient of 560° C to 500° C. This leads to the growth of $0.5 \times 1 \times 1$ mm^3 large B20 FeGe crystals at the lower temperature side. The B20 crystal structure was confirmed by powder X-ray diffraction (see Supplementary Fig. S???) and surfaces for MFM imaging were oriented using Laue diffraction.

The data that support the plots within this paper and other findings of this study are available from the corresponding authors upon request.

References

1. Chuang, I., Durrer, R., Turok, N. & Yurke, B. Cosmology in the Laboratory: Defect Dynamics in Liquid Crystals. *Science* **251**, 1336–1342 (1991).

2. del Campo, A. & Zurek, W. H. Universality of phase transition dynamics: Topological defects from symmetry breaking. *Inter. J. Mod. Phys. A* **29**, 1430018 (2014).

3. Catalan, G., Seidel, J., Ramesh, R. & Scott, J. F. Domain wall nanoelectronics. *Rev. Mod. Phys.* **84**, 119–156 (2012).

4. Parkin, S. S. P., Hayashi, M. & Thomas, L. Magnetic Domain-Wall Racetrack Memory. *Science* **320**, 190–194 (2012).

5. Salje, E. & Zhang, H. Domain boundary engineering. *Phase Transit.* **82**, 452–469 (2009).

6. Yu, X. Z. *et al.* Real-space observation of a two-dimensional skyrmion crystal. *Nature* **465**, 901–904 (2010).

7. Yu, X. Z. *et al.* Near room-temperature formation of a skyrmion crystal in thin-films of the helimagnet FeGe. *Nat. Mat.* **10**, 106-109 (2011).

8. Bak, P. & Jensen, M. H. Theory of helical magnetic structures and phase transitions in MnSi and FeGe. *J. Phys. C: Solid State Phys.* **13**, L881 (1980).

9. de Gennes, P. G. & Prost, J. *The Physics of Liquid Crystals* (Clarendon, Oxford, 1993).

10. Hubert, A. & Schäfer, R. *Magnetic Domains: The Analysis of Magnetic Microstructures* (Springer, Berlin Heidelberg, 2009).

11. Kléman, M. Magnetic singularities in helimagnet crystals, *Phil. Mag.* **22:178**, 739–749 (1970)

12. Seul, M., Monar, L. R., O'Gorman, L. & Wolfe, R. Morphology and Local Structure in Labyrinthine Stripe Domain Phase. *Science* **254**, 5038 (1991).

13. Uchida, M. *et al.* Topological spin textures in the helimagnet FeGe. *Phys. Rev. B* **77**, 184402 (2008).

14. Li, F., Nattermann, T. & Pokrovsky, V. L. Vortex domain walls in helical magnets. *Phys. Rev. Lett.* **108**, 107203 (2012).

15. Lebech, B., Bernhard, J. & Freltoft, T. Magnetic structures of cubic FeGe studied by small-angle neutron scattering. *J. Phys.: Condens. Matter* **1**, 6105 (1989).

16. Rybakov, F. N., Borisov, A. B., Blügel, S. & Kiselev, N. S. New spiral state and skyrmion lattice in 3D model of chiral magnets. *New J. Phys.* **18**, 045002 (2016).

17. Yagil, A. *et al.* Stray field signatures of Néel textured skyrmions in Ir/Fe/Co/Pt multilayer films. Preprint at https://arxiv.org/abs/1705.07608 (2017).

18. Bouligand, Y. *Dislocations in Solids* Ch. 23 (North-Holland Publishing Company, New York, 1983).

19. Bouligand, Y. Recherches sur les textures des états mésomorphes. 3. Les plages à éventails dans les cholestériques. *J. Phys. France* **34**, 603–614 (1973).

20. Bouligand, Y. Recherches sur les textures des états mésomorphes. 4. La texture à plans et la morphogenèse des principales textures dans les cholestériques. *J. Phys. France* **34**, 1011–1020 (1973).

21. Nagaosa, N. & Tokura, Y. Topological properties and dynamics of magnetic skyrmions. *Nature Nanotech.* **8**, 899–911 (2013).

22. Garst, M. in *Topological Structures in Ferroic Materials* (Springer International Publishing 2016).

23. Neubauer, A. *et al.* Topological Hall Effect in the A Phase of MnSi. *Phys. Rev. Lett.* **102**, 186602 (2009).

24. Schulz, T. *et al.* Emergent electrodynamics of skyrmions in a chiral magnet. *Nat. Phys.* **8**, 301–304 (2012).

25. Schütte, C. & M. Garst, M. Magnon-skyrmion scattering in chiral magnets. *Phys. Rev. B* **90**, 094423 (2014).

26. Mochizuki, M. *et al.* Thermally driven ratchet motion of a skyrmion microcrystal and topological magnon Hall effect. *Nat. Mat.* **13**, 241–246 (2014).

27. A. Bauer, A. Chacon, M. Wagner, M. Halder, R. Georgii, A. Rosch, C. Pfleiderer, and M. Garst, Symmetry breaking, slow relaxation dynamics, and topological defects at the field-induced helix reorientation in MnSi. Phys. Rev. B **95**, 024429 (2017).

28. Dussaux, A. *et al.* Local dynamics of topological magnetic defects in the itinerant helimagnet FeGe. *Nat. Commun.* **7**, 12430 (2016).

29. Janoschek, M. *et al.* Fluctuation-induced first-order phase transition in Dzyaloshinskii-Moriya helimagnets. *Phys. Rev. B* **87**, 134407 (2013).

30. H. Wilhelm, H. *et al.* Precursor phenomena at the magnetic ordering of the cubic helimagnet FeGe. *Phys. Rev. Lett.* **107**, 127203 (2011).

31. Pfleiderer, C., Julian, S. R. & Lonzarich, G. G. Non-Fermi-liquid nature of the normal state of itinerant-electron ferromagnets. *Nature* **414**, 427–430 (2001).

32. Ritz, R. *et al.* Formation of a topological non-Fermi liquid in MnSi. *Nature* **497**, 231–234 (2013).

33. Pedrazzini, P. *et al.* Metallic state in cubic FeGe beyond its quantum phase transition. *Phys. Rev. Lett.* **98**, 047204 (2007).

34. Fert, A., Cros, V. & Sampaio, J. Skyrmions on the track. *Nature Nanotech.* **8**, 152–156 (2013).

35. Wiesendanger, R. Nanoscale magnetic skyrmions in metallic films and multilayers: a new twist for spintronics. *Nat. Rev. Mater.* **1**, 16044 (2016).

Acknowledgement We thank M. Fiebig for direct financial support. The work at ETH was supported by the Swiss National Science Foundation through grants 200021-149192, 200021-137520. L.K. and M.G. were supported by SFB 1143 ”Correlated Magnetism: From Frustration To Topology” and DFG grant GA 1072/5-1. J.M. and A.R. were supported by SFB 1238 (Kontrolle und Dynamik von Quantenmaterialien). J.M. also acknowledges support from the Deutsche Telekom Stiftung and Bonn-Cologne Graduate School of Physics and Astronomy BCGS. N.K. acknowledges funding through the JSPS Grant-in-Aids for Scientific Research (S) No. 24224009 and for Young Scientists (Start-up) No. 26886005. D.M. thanks the Research Council of Norway (FRINATEK project no.263228) and Norwegian University of Science and Technology (NTNU) for financial support.

Author Contributions P.S. conducted the MFM experiments supervised by D.M.; J.M.performed the 2D micromagnetic simulations supervised by M.G. and A.R.; N.K. grew the FeGe single crystals under supervision of Y.T; P.S., J.M., L.K., M.G. and D.M. classified the domain walls; M.G. and L.K. defined the skyrmion charge of edge dislocations; P.S., J.M., L.K., M.G. and D.M. wrote the paper; M.G. and D.M. supervised the work. All authors discussed the results and contributed to their interpretation.

Competing financial interests The authors declare that they have no competing financial interests.

Supplementary Information is linked to the online version of the paper at www.nature.com/nature.

Figure 1

Helimagnetic order and defect structures. **a,** Right-handed magnetic helix. **b,** Magnetic moments form periodic layers (black arrows) orthogonal to the helix axis $\mathbf{Q}$. Bright and dark areas corresponds to stray fields pointing in and out of the plane, respectively. **c,** π disclination. **d,** $-\pi$ disclination. **e,** Edge dislocation formed by a pair of π and $-\pi$ disclinations at distance D. The Burgers vector, $B = 2D$, is given by an integer multiple of the helix wavelength, $B = n\lambda$ (here, $n = 2$).

Figure 2

Helimagnetic domain walls in FeGe. **a,** Curvature wall (type I). **b,** Zig-zag disclination wall (type II). **c,** Dislocation wall (type III). The MFM data is obtained at 260-273 K. **d,** Quantitative analysis of the domain wall angle α (see **a-c**) as function of the angle between $\mathbf{Q}_1$ and $\mathbf{Q}_2$ ($\angle(\mathbf{Q}_1, \mathbf{Q}_2)$, defined in **a**). The plot reveals three distinct stability regimes for type I (red), type II (blue), and type III (green) walls. Special type II walls (light-blue) occur in the transition regions (see inset images) as explained in detail in the main text. Within the marked region in **c** (white dashed contour) the wall changes from type III to type I.

Figure 3

Micromagnetic domain wall simulations. Energy per length of **a,** type I,**b,c,** type II, and **c-g,** type III walls, where A is the exchange energy. The graph shows that type I walls are lowest in energy density for small angles $\angle(\mathbf{Q}_1, \mathbf{Q}_2)$. Type II walls stabilize for intermediate angles. As $\angle(\mathbf{Q}_1, \mathbf{Q}_2)$ increases, type II walls with smaller defect distance D become energetically favourable (blue, numbers in units of $\lambda/2$). For larger angles, type III walls with continuous stripes ($B = 3\lambda$ (dark green line), 2λ (**d**) and λ (**e**) are most stable. The associated Burgers vector varies with $\angle(\mathbf{Q}_1, \mathbf{Q}_2)$ (green, numbers in units of λ).

Figure 4

Magnetic edge dislocation with nonzero skyrmion charge. a, Magnetic skyrmion with topological charge $W = -1$, **b,** Cartoon of a skyrmion embedded in a helimagnetic background, **c, d,** Cartoon and spin configuration of an edge dislocation with Burgers vector $B = \lambda$, i.e., a meron with $W = -\frac{1}{2}$. **e,** Illustration of the spin structure of a type II domain wall with $D = 3\lambda/2$.

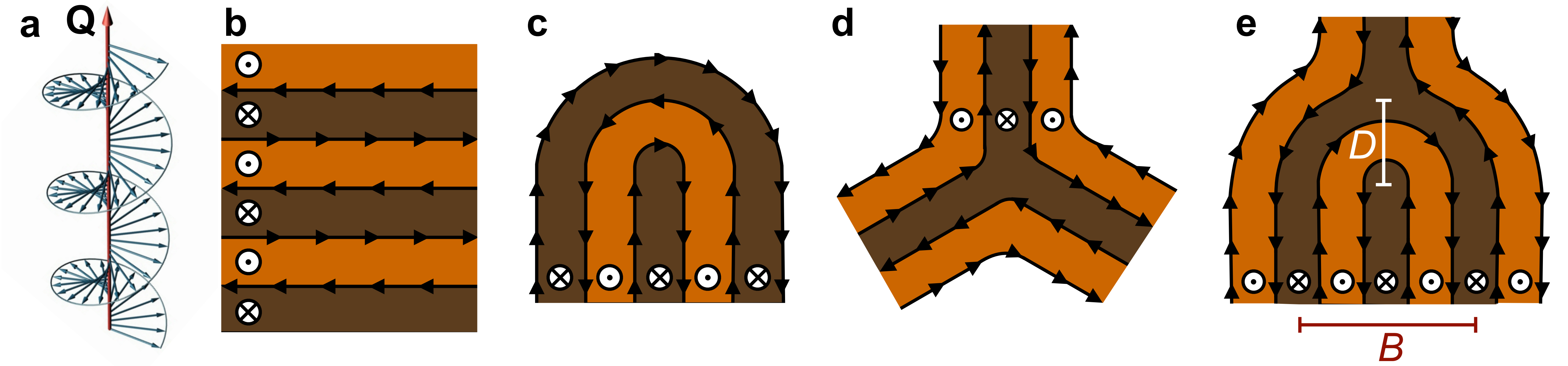

a
Q
b
c
d
e
D
B

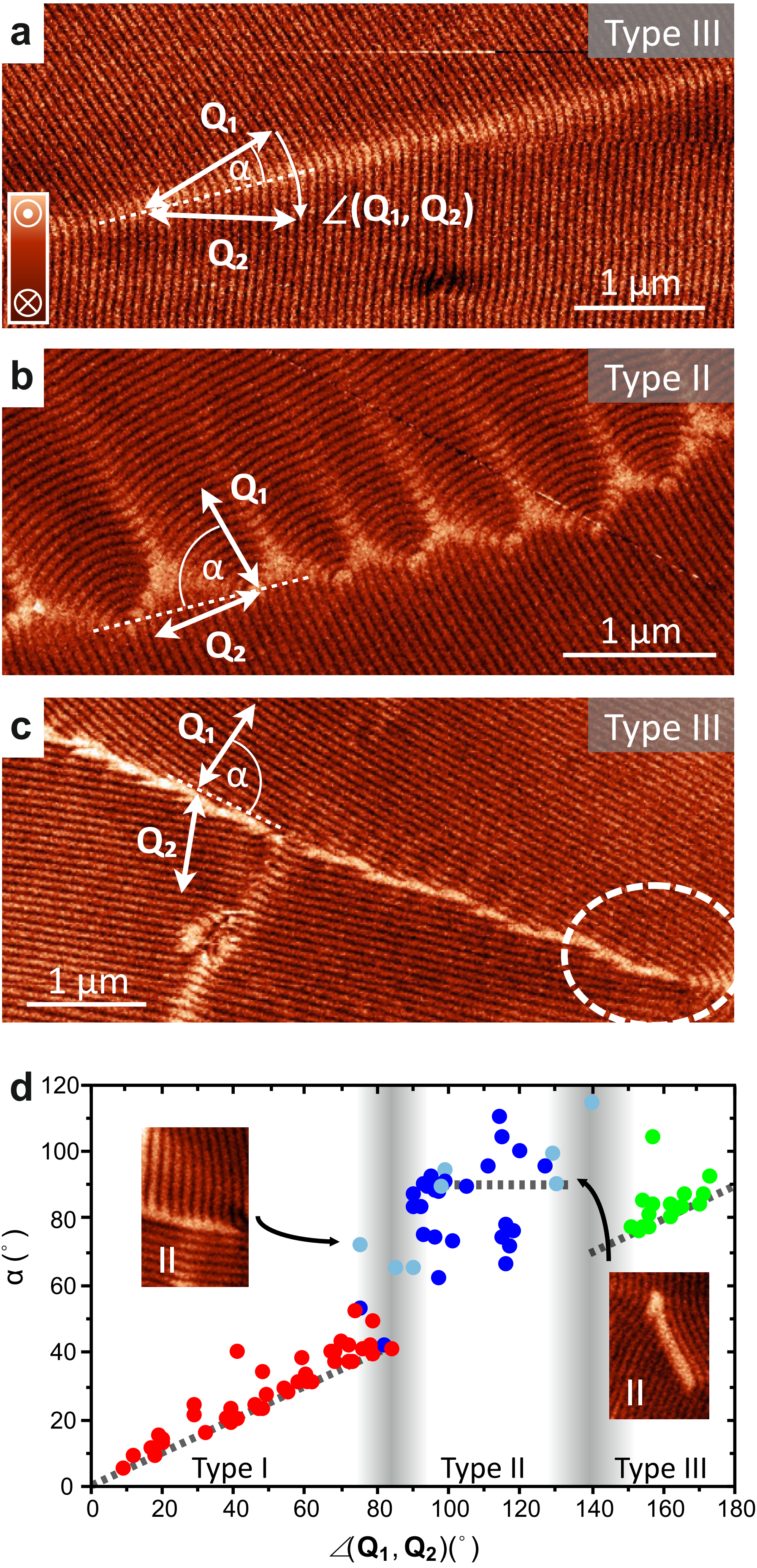
a
Type III
Q1
α
∠(Q1, Q2)
Q2
1 μm
b
Type II
Q1
α
Q2
1 μm
c
Type III
Q1
α
Q2
1 μm
d
α (°)
∠(Q1, Q2)(°)
II
II
Type I
Type II
Type III
0
20
40
60
80
100
120
140
160
180

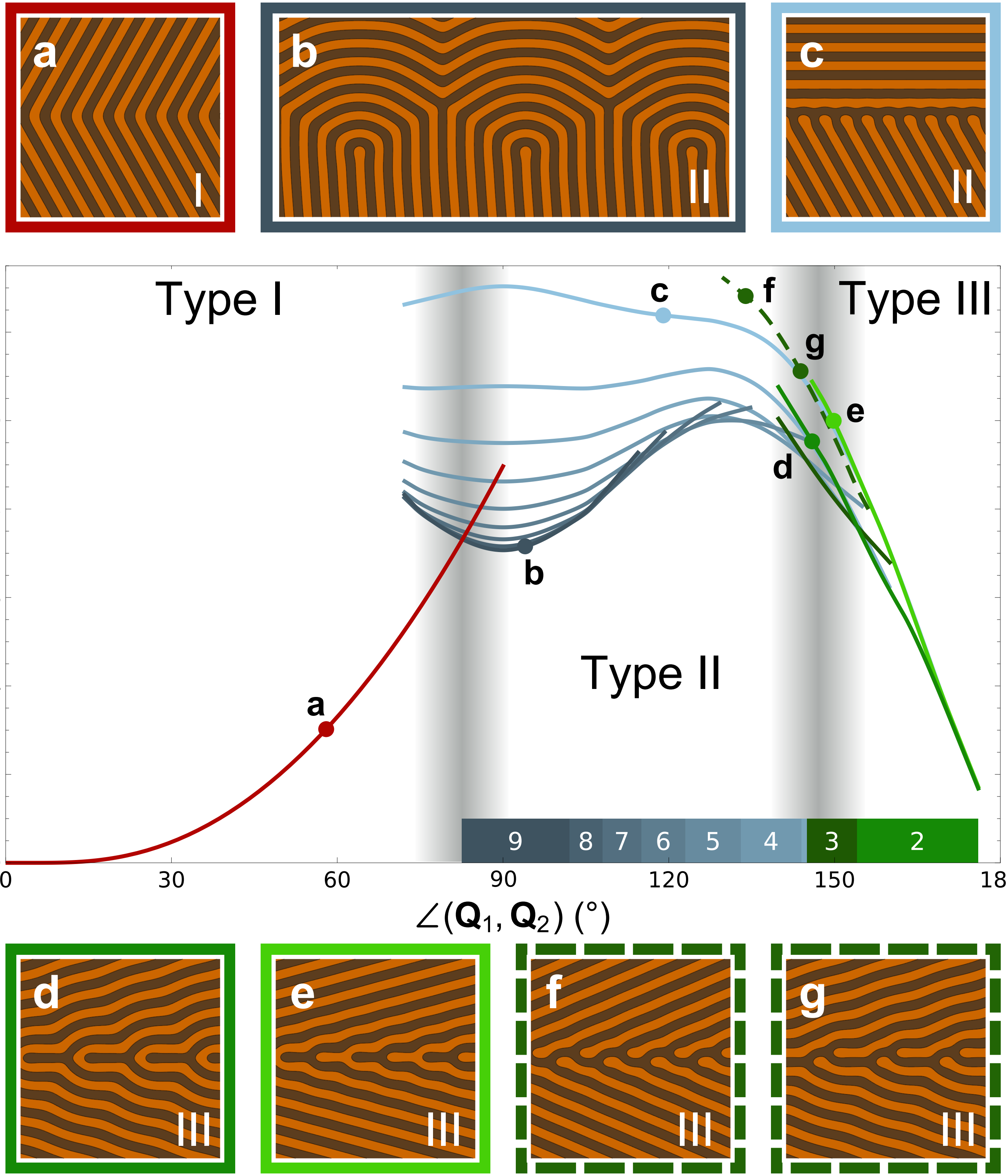

a
I
b
II
c
II
Type I
Type II
Type III
Domain wall energy density (2A/λ)
∠(Q1, Q2) (°)
9
8
7
6
5
4
3
2
d
III
e
III
f
III
g
III

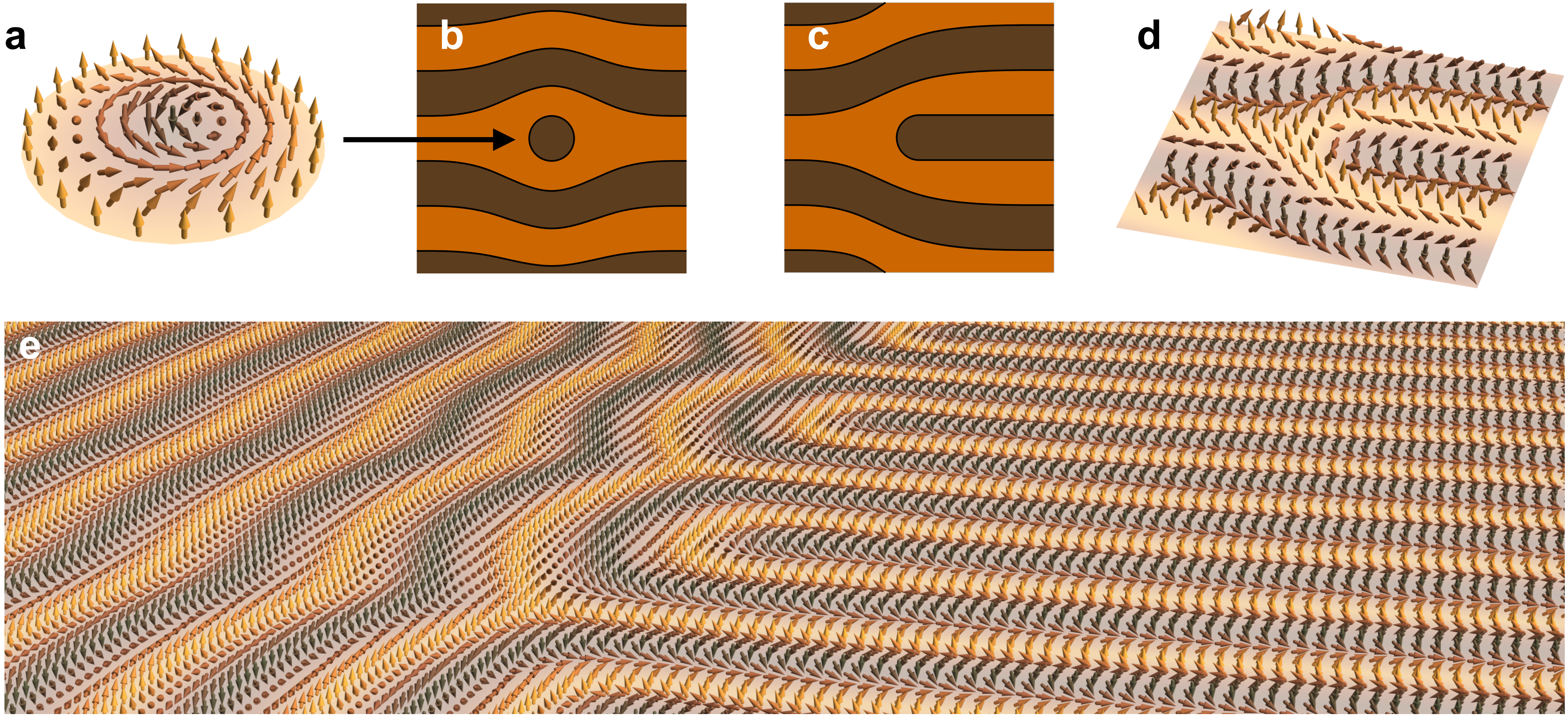

a
b
c
d
e